communications biology

A Nature Portfolio journal

Article

https://doi.org/10.1038/s42003-025-08081-0

Evidence for a push-pull interaction between superior colliculi in monocular dynamic vision mode

Check for updates

Rita Gil, Mafalda Valente, Francisca F. Fernandes & Noam Shemesh ✉

Visual perception can operate in two distinct vision modes—static and dynamic—that have been associated with different neural activity regimes in the superior colliculus (SC). However, the associated pathway-wide mechanisms remain poorly understood, especially in terms of corticotectal and tectotectal feedback upon encoding the continuity illusion during the dynamic vision mode. Here, we harness functional MRI combined with rat brain lesions to investigate whole-pathway neural interactions in the dynamic vision mode. We find a push-pull mechanism embodying contralateral suppression of SC activity opposing positive ipsilateral neural activation upon monocular visual stimulation. Cortical amplification is confirmed through cortical lesions, while further lesioning the ipsilateral SC leads to a boost in the contralateral SC negative signals, suggesting a tectal origin for the push-pull interaction. These results highlight hitherto unreported frequency-dependent modulations in the tectotectal pathway and further challenge the notion that intertectal connections solely serve as reciprocal inhibitory mechanisms for avoiding visual blur during saccades.

The rapid assessment of the surrounding environment and appropriate behavioural response to external stimuli (e.g. to approach, avoid or ignore) is key for animal survival[1]. The continuity illusion is a perceptual feature enabling the brain to interpret moving surroundings smoothly and detect new emerging features in a continuously stable environment. When observing a flickering light, when the frequency of the light reaching the retina is low, each flash is perceived as unique and the system operates in static vision mode; if the temporal frequency of the stimulus is above the flicker fusion frequency (FFF) threshold, the system operates in the dynamic vision mode where the stimuli are fused to an illusory continuous percept.

The superior colliculus (SC) is an important relay for sensory pathways (e.g. visual, auditory and somatosensory) with several outputs towards motor areas[2] and it is known to play critical roles in multimodal integration and rapid sensorimotor transformation[3–5]. Cells in the SC superficial visual layers (sSC) are imperative for visual saliency detection[3,6–8], i.e. stimulus appearance/disappearance or movement (important for innate defensive responses such as escape or camouflage from predators). Importantly, the SC activity was found to strongly depend on flashing stimulus frequency associated with the encoding of the response habituation (RH) phenomenon[9,10] characterised by response decrements, both in total number of spikes[6] and local field potentials (LFPs) N1-P1 amplitude attenuation[11], to repeated stimuli presentations. RH has been thought of as a form of short-term memory for familiar versus novel information based on a dynamic adjustment of response thresholds. This phenomenon also linked SC with novelty detection, and was shown to be underpinned by multiple inhibitory feedback mechanisms[12,13] occurring between and within the two SCs: the coactivation of excitatory and inhibitory neurons would lead to a long-lasting inhibition that would block responses to subsequent stimulus at sufficiently high frequencies. In higher-order primates and humans, the higher visual cortical areas have been more implicated with visual perception. However, the role of SC as 'novelty detector' along with other rodent collicular properties usually associated with cortical regions of primates (such as orientation selectivity[14]), suggests a more prominent role of the SC alongside the visual cortex (VC) in rodent visual processing. A recent study encompassing behavioural readouts, functional MRI (fMRI), and electrophysiology in the rat animal model found the most marked correlation with flashing stimuli frequency occurring at the level of the SC, where transitions between activation and suppression states matched the behaviourally reported FFF threshold, where the shift from static to dynamic vision modes takes place[15]. Interestingly, the SC fMRI signals also revealed the expected characteristics of 'novelty detection', i.e. strong flash-induced positive signals in low frequency stimulation (representing the novelty introduced by each flash) and onset/offset positive peaks surrounding the stimulation period in the dynamic vision mode (representing the novelty of brightness changes since the stimulus is perceived as a continuous light).

The SC is positioned strategically in the midbrain (Fig. 1A), and its high connectivity[2–5] with other areas suggests a potential role for inter-area interactions that could contribute to the encoding and operation of the

Champalimaud Research, Champalimaud Foundation, Lisbon, Portugal. ✉e-mail: noam.shemesh@neuro.fchampalimaud.org

vision modes. In the rodent brain, around 85-90% of retinal ganglion cells (RGCs) project directly to the sSC. As retinal evoked potentials can still track individual light flashes during the dynamic vision mode[16,17], the SC activity modulation is potentially impacted by feedback arriving to the region. Several feedback connections are known, mainly from the ipsilateral primary visual cortex (V1) through corticotectal connections[3,15,18–20] and from the contralateral SC (cSC) through intertectal connections[4,5,21]. Corticotectal connections project to all layers of the SC and are known to be aligned with retinal inputs. These connections are thought to exert a gain control effect on tectal cells: sSC neurons inherit feature selectivity from retinal hardwired circuits and modulate their response magnitude depending on cortical input that may be subject to modulation by, for example, the animal's internal state, attention and learning[3,15,18–20]. Reduced responsiveness in many sSC neurons has been reported after inactivation of corticotectal feedback connections, either by cortical removal, pharmacological depression, optogenetic silencing or cooling[19,20,22–25]. Tectotectal connections between the two superior colliculi are also known to play important roles in visual-orienting behaviours[26]: the two SCs are connected through commissural fibres thought to be responsible for a reciprocal intertectal inhibitory effect[18,27–31] related to surround inhibition and to suppression of visual inputs during saccades which would otherwise lead to visual blur[1]. The existence of direct inhibitory connections between the cSC and ipsilateral SC (iSC) was confirmed by intracellular recordings of inhibitory postsynaptic potentials from collicular cells in response to electrical stimulation of the cSC[30]. Although most electrophysiological studies support a predominantly inhibitory intertectal effect, evoked activation in several tectal cells after stimulation of intertectal fibres has also been reported[7,26,27].

Studies of corticotectal and tectotectal connections have been performed in the static vision mode, where SC activation is expected to occur following a visual stimulus. However, how the two colliculi interact between themselves and with other areas during the dynamic vision mode is still poorly understood. Here, we harness fMRI, which allows for a whole-pathway perspective, and brain lesions in key visual pathway structures (Fig. 1A), to investigate collicular interactions and the impact of corticotectal and tectotectal feedback in the observed SC neural suppression in the dynamic vision mode. A monocular stimulation regime (Fig. 1B, C) was used to actively isolate activity derived from the visual stimulus into one hemisphere and to allow the investigation of interhemispheric tectal connections. We discover a push-pull interaction between the two SCs during the dynamic vision mode upon monocular stimulation, pointing at the role of tectotectal feedback beyond general reciprocal inhibition.

Results

Opposing tectal responses in the monocular dynamic vision mode

We first examined the overall temporal profile of fMRI signals in regions of interest (ROIs) placed along the visual pathway (Fig. 2 and Supplementary Fig. 1). Monocular stimulation at 1 Hz (Fig. 2A) revealed positive blood oxygenation level dependent (BOLD) responses in both cortical and subcortical visual structures with increased percentage of signal change in the contralateral hemisphere as expected from the monocular nature of the visual stimulus. Raw signals from entire runs for the different ROIs show no habituation effects along the different stimulation blocks and further confirm the high data quality (Supplementary Figs. 1 and 2).

On the other hand, visual stimulation at 25 Hz evoked negative bilateral cortical and cSC responses along with positive thalamic and positive iSC responses (Fig. 2B, Supplementary Figs. 1 and 2).

During the dynamic vision mode, cSC responses could be clearly divided into three distinct periods: two positive 'peaks', at the beginning and after the end of the visual stimulation period (hereafter referred to as onset and offset peaks, respectively, and highlighted by dashed arrows in Fig. 2B), and a strong negative fMRI signal in-between (hereafter referred to as the ON period, and highlighted by a solid arrow in Fig. 2B). Unlike the strong negative signal during the ON period in the cSC, the iSC evidenced positive fMRI responses with less clear (if any) distinction between onset/ON/offset periods. Still at the subcortical level, positive signals were noted in the lateral geniculate thalamic nucleus (LGN) for both hemispheres (with reduced percentage of signal change for the ipsilateral hemisphere, as expected from the monocular nature of the visual stimulus). Although not as prominent as in the SC, the three periods could be somewhat discerned in the contralateral LGN responses (Fig. 2B, middle panel, and highlighted by black arrows). At the cortical level, monocular stimulation induced strong bilateral negative signals in the V1, with stronger negative responses observed in the contralateral hemisphere. The three periods observed in the contralateral responses at the subcortical level were not distinguishable in the cortical responses. Although an onset was not evident, the peak cortical signal coincided with the subcortical ON periods (filled black arrow in the V1 time profile of Fig. 2B at ~6 s after stimulus started), and a more conventional post-stimulation signal (in this case, overshoot) was observed (dashed black arrow in the V1 time profile of Fig. 2B).

To understand the spatial distribution of the fMRI signals during both vision modes, a conventional general linear modelling (GLM) analysis tracking the whole stimulation block paradigm was first performed for the two vision modes (Fig. 2C). The corresponding t-maps highlighted the positive (mostly) contralateral cortical and subcortical responses during the static vision mode. By contrast, for the dynamic vision mode, bilateral cortical negative fMRI activation centred in the V1, with a larger activation extent in the contralateral hemisphere was observed. Still during the dynamic vision mode, at the subcortical level, opposing polarity SC responses were clearly observed: in the ipsilateral side, positive activation spanning the entire medial SC plane was noted, while the cSC activation was clearly negative and appeared localised in more medial cSC regions. In the LGN, positive activation covering the entire structure was observed, with higher t-values in the contralateral hemisphere.

The SC time profiles during the dynamic vision mode, seen in Fig. 2B, suggest that a multi-periodic analysis may be more relevant to decompose the activation in the onset, ON, and offset epochs, respectively (Fig. 2D). Under this analysis, onset t-maps revealed that the onset peaks are localised only at the subcortical structures forming the parallel streams of the visual pathway - no activation could be detected for the onset signal in the cortical areas. The ON period t-maps strongly highlighted the opposite polarity of tectal responses: negative signals in cSC and positive signals in iSC. These maps further confirm that contralateral responses cover more medial and dorsal regions of the cSC while the positive ipsilateral responses span the entire medial-lateral extent of the iSC. The ON period t-maps also demarcate the negative bilateral V1 responses during the dynamic vision mode. LGN ON signals are positive with a similar spatial distribution as LGN onset signals. Offset t-maps show positive activation for subcortical structures, with the largest t-values in cSC. Particularly for the cSC, the offset signal spatial distribution covers the entire structure similarly to the onset t-maps. Offset signals in LGN appear to be more localised in the outer shell of this structure. Finally, negative contralateral offset signals appear for the V1 region which reflect the recovery of cortical signals to baseline.

Diminished V1 feedback decreases cSC onset activation and ON suppression responses during the dynamic vision mode

To reduce corticotectal feedback, the V1 was bilaterally lesioned (histological images revealing the loss of tissue integrity and sparser cell density in the lesioned areas at scanning time are shown in Supplementary Fig. 3) and experiments were repeated (Fig. 3A–C). Observing individual and averaged time series after V1 lesioning (Supplementary Fig. 2) also revealed no short-term habituation effects to the visual stimulus. The responses in both SCs for this group are shown in Fig. 3A (time profiles of other visual pathway structures can be seen in Supplementary Fig. 4A). In the cSC time profiles, the amplitude decreases were observed in the onset peak and ON periods. The cSC response (Fig. 3A, solid blue line) was less negative compared to its control counterpart (Fig. 3A, dashed blue line). The direction of the response is marked with a solid blue arrow in Fig. 3A.

GLM maps calculated for the onset, ON and offset periods, revealed interesting spatial distribution patterns (Fig. 3B shows the slice capturing

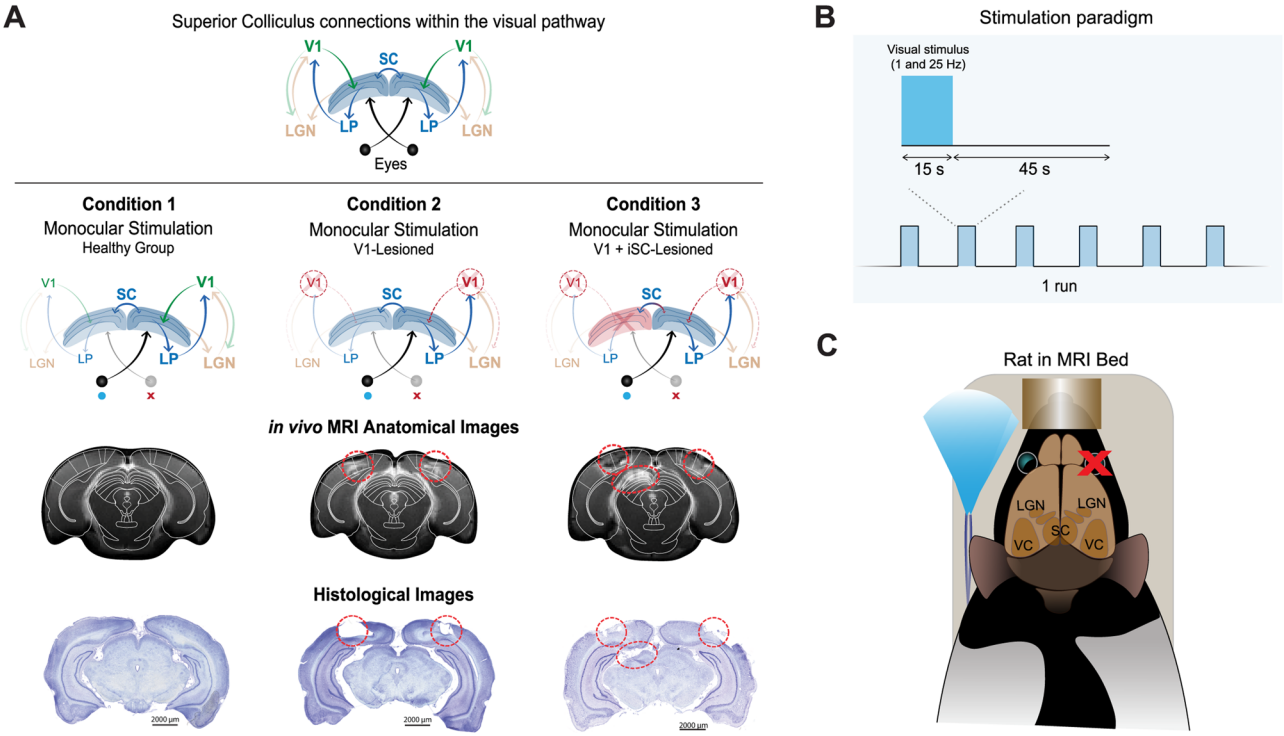

Fig. 1 | Experiment schematics. A Schematic of the rat visual pathway and different tested conditions: Healthy group where no lesions were performed; V1-lesioned group where corticotectal feedback is reduced due to bilateral lesions in the V1; and V1+iSC-lesioned group where corticotectal and tectotectal feedback is reduced through bilateral lesions in the V1 combined with unilateral lesions in the iSC. MRI and histological images confirm the correct placement of the lesions for specific feedback reduction; **B** Stimulation paradigm consisting of 15 s of a flashing visual stimulus (frequencies = 1 and 25 Hz) to induce the static and dynamic vision modes, followed by 45 s of rest. Each experimental run consisted of six repetitions of the described stimulation block; **C** Schematic of the animal in the MR bed with the LED tip placed in front of one eye while the other eye was covered for efficient monocular stimulation. V1 primary visual cortex; iSC ipsilateral superior colliculus.

most of the SC; other slices containing SC are shown in Supplementary Fig. 4B). Similar to the healthy group (e.g. maps in Fig. 2D), the V1-lesioned group exhibited strong positive onset activation in both SCs (Fig. 3B). The opposing ON responses of the cSC and iSC, with weaker negative values in more medial cSC regions, and similarly positive values in the iSC areas, remained visible. Offset signals were confined to the cSC.

To obtain a more quantitative assessment of how cortical lesions affected activity in the tectum, difference t-maps were calculated for each signal period, representing the statistical differences (t-values) between the V1-lesioned group and the healthy animals (Fig. 3C, other slices containing SC are shown in Supplementary Fig. 4C). In this fixed-effects analysis, greener colours represent statistically negative differences between the groups, and warmer colours represent statistically positive differences. For both the onset and ON t-maps, a clear difference in t-values was observed in the more medial superficial cSC regions, with negative onset difference t-values (representing the decrease in the onset peak amplitude as seen in time profiles) and positive ON difference t-values (representing the less negative ON period amplitude after cortical lesioning). The offset signals showed no differences between the two groups. Similar experiments for the static vision mode are reported in Supplementary Figs. 5 and 6.

Further lesioning iSC boosts cSC suppression in the dynamic vision mode

To dissect the role of intertectal connections in the push-pull interaction observed above, and to avoid cortical loop effects, a third group was lesioned bilaterally in both the V1 (abolishing cortical feedback) and in the iSC (abolishing tectotectal feedback). Figure 3D shows ROI time profiles for this group (time profiles of other visual pathway structures can be seen in Supplementary Fig. 4D), represented by filled lines, revealed the expected flat ipsilateral tectal responses (Fig. 3D, solid yellow line; the V1-lesioned response is shown for comparison in the dashed yellow line), confirming the effectiveness of the iSC lesion.

In the cSC, we find a starkly more negative response for the V1+iSC lesioned group (Fig. 3D, solid blue line; the V1-lesioned response is in dashed blue for comparison). Interestingly, the onset peak is not markedly changed, while the offset peak is somewhat weaker than in the V1-lesioned group. The corresponding t-maps (Fig. 3E, other slices containing SC are shown in Supplementary Fig. 4E) reveal that onset signals, similarly to offset signals, were circumscribed to the superficial cSC layers and spanned the entire medial plane of the structure. The ON t-maps evidenced strong negative values along the entire cSC and no positive iSC (lesioned) responses.

As above, we assess the differences more quantitatively via difference maps (Fig. 3F, other slices containing SC are shown in Supplementary Fig. 4F). The decrease in the iSC responses was evidenced both in onset and ON difference maps. The onset maps reveal no differences in the onset cSC signals of both groups. The ON difference maps further revealed significantly more negative responses in cSC. Offset t-maps evidenced a small decrease in offset signals at the superficial cSC layers. Similar experiments for the static vision mode are reported in Supplementary Figs. 5 and 6.

Discussion

The visual pathway switches between the static and dynamic vision modes, depending on the frequency of stimulus presentation, to encode for temporal stability and detect novel features in the surrounding environment. The rat SC, known for its involvement in RH[6,9–13] and novelty detection[3,6–8], has been recently implicated in the encoding of the transitions between these vision modes[15]. At frequencies lower than the FFF threshold, every stimulus elicits increased population-level activity in the SC including elevated LFPs and multi-unit activity (MUA)[15,32,33], and the system operates in the static vision mode. In particular, RH (characterised by a decrease of SC activity)

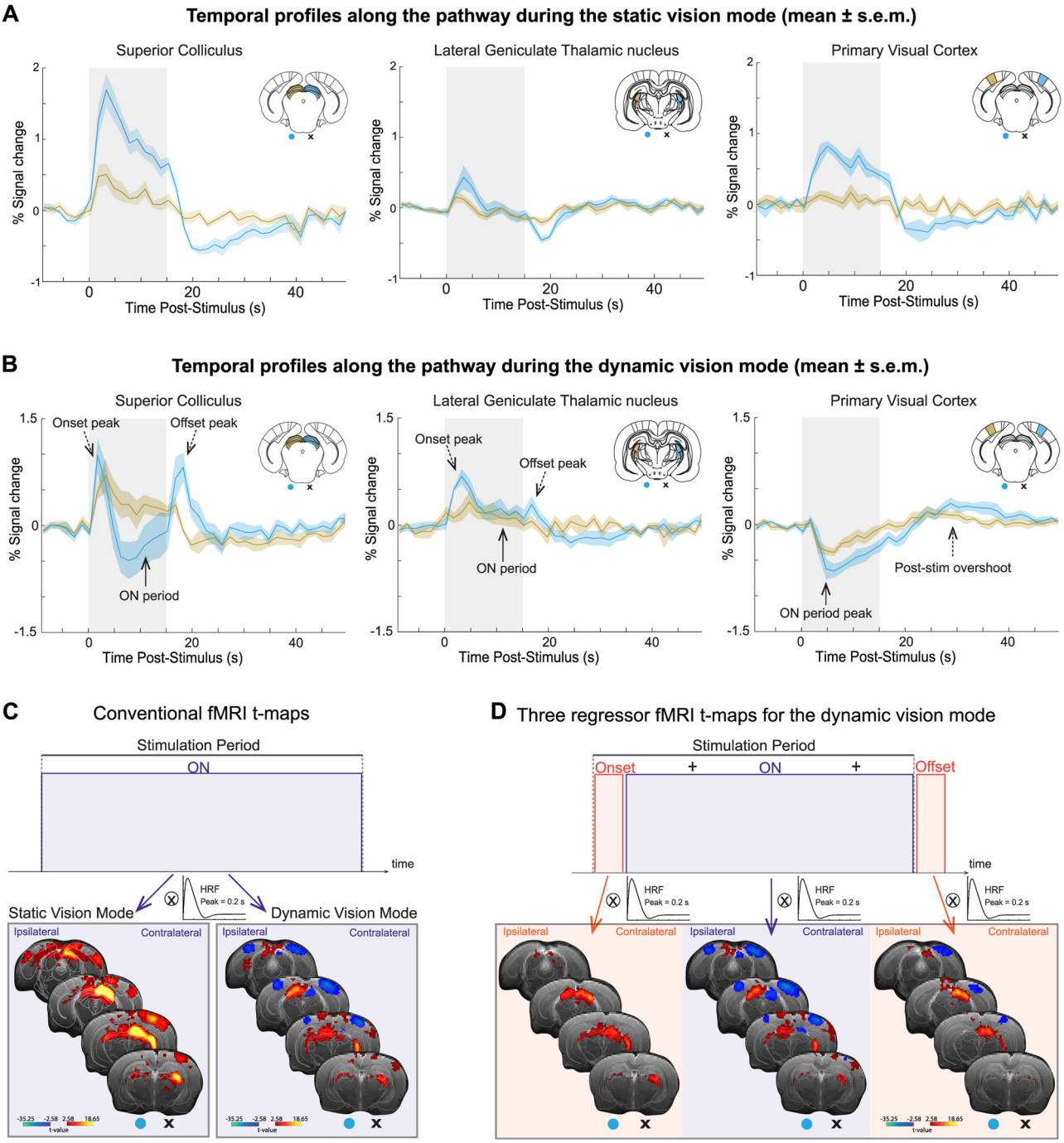

Fig. 2 | fMRI responses for the healthy group during the static and dynamic vision modes. Temporal profiles of the three main structures of the visual pathway - SC, LGN and V1 - for the static (**A**) and dynamic (**B**) vision modes. Responses for the contralateral and ipsilateral hemispheres are shown in blue and yellow, respectively. While in the static vision mode contralateral visual pathway structures reveal positive BOLD responses with increased percent signal change when compared to the ipsilateral counterparts (as expected from the monocular stimulation regime), in the dynamic vision mode contralateral multi-periodic responses can be observed in subcortical structures, particularly within the SC. Black arrows point to the 3 detected periods of the response: onset peak (dashed arrow), ON period (full arrow) and offset peak (dashed arrow). Cortical responses have ON period peak and post-stim overshoot marked with filled and dashed black arrows, respectively; **C** fMRI t-maps assuming one regressor for the entire stimulation period. On the left side, t-maps from the static vision mode confirm the positive responses along the visual pathway with larger t-values in the contralateral hemisphere. On the right side, negative cortical responses along with opposing tectal responses and positive contralateral LGN responses can be observed in the dynamic vision mode; **D** Decomposition of the stimulation block into 3 periods corresponding to the onset/ON/offset periods of the responses seen during the dynamic vision mode. Onset and offset t-maps are highlighted in orange and the ON period t-map is highlighted in dark purple. The left side of the t-maps represents the ipsilateral hemisphere while the right side represents the contralateral hemisphere. T-maps were tested for a minimum significance level of 0.005 with a minimum cluster size of 10 voxels and corrected for multiple comparisons using a cluster false discovery rate test. SC superior colliculus, LGN lateral geniculate thalamic nucleus, V1 primary visual cortex.

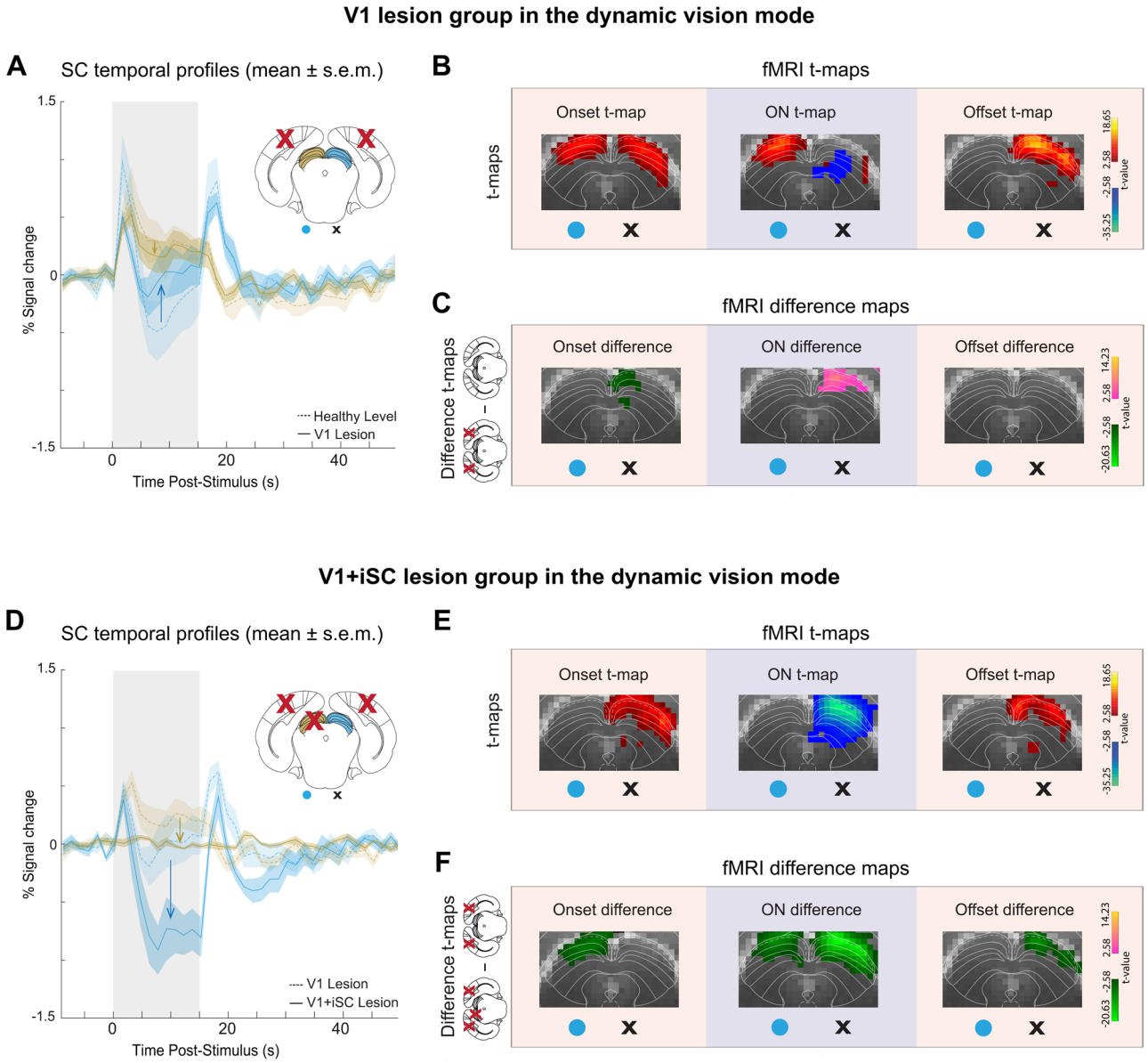

Fig. 3 | SC fMRI responses for the lesioned groups during the dynamic vision mode. A–C V1-lesioned group and **D–F** V1+iSC-lesioned group responses. **A**, **D**: SC time profiles for the contralateral (blue) and ipsilateral (yellow) hemispheres. The healthy group and V1-lesioned responses are shown in dashed lines for clearer comparison in **A**, **D**, respectively; **B**, **E** Decomposition of the responses into the three detected periods (onset/ON/offset) and t-maps for each period. Onset and offset t-maps are highlighted in orange and the ON period t-map is highlighted in dark purple; **C**, **F** Difference maps for each response period. The left side of the maps represents the ipsilateral hemisphere while the right side represents the contralateral hemisphere. T-value maps were thresholded with $p < 0.005$ and a minimum cluster size of 10 voxels, and were cluster-FDR corrected at $p < 0.005$, both when analysing each group and the difference between groups. V1 primary visual cortex, iSC ipsilateral superior colliculus.

progressively occurs in the SC as the inter-stimulus interval between light flashes decreases. In other words, stronger RH occurs as the stimulation frequency increases. As stimulation frequency increases beyond the FFF threshold, stimuli become fused and the neural activity in the SC is generally suppressed, entering the dynamic vision mode, with two exceptions: onset and offset signals clearly appear at the edges of the stimulation period, associated with the novelty of the initial transition from dark to bright in the very beginning of stimulation, as well as with the sharp transition from light back to darkness in the very end of the stimulation, each eliciting a novelty detection by SC[15,34] (*vide infra*). This dual action, of encoding novelty by eliciting activity in SC and silencing SC beyond the FFF threshold, suggests different SC modes of operation and potentially different interactions with other brain structures and even within the two superior colliculi. In the static vision mode, corticotectal projections are known to have a gain effect over the SC's activity. Most studies suggested that these connections facilitate SC responses during the static vision mode[19,20,22–24,35]. Intertectal SC connections, associated with reduction of saccadic blur and visual-orienting behaviours through the 'Sprague effect'[29], have been mostly assumed to be inhibitory.

In the dynamic vision mode, less is known about the tectotectal and corticotectal interactions, motivating our current work. To investigate these interactions, we chose to harness fMRI due to its ability to noninvasively provide a whole-pathway overview of population level activity in the system (n.b. the excellent correlation between population-level activity - MUA - and fMRI signals observed recently under similar conditions[15,34]) along with brain lesions in bilateral cortical and unilateral SC areas that allow the abolishment of specific inputs into the SC. We further opted for monocular stimulation to isolate the role of each SC at a time.

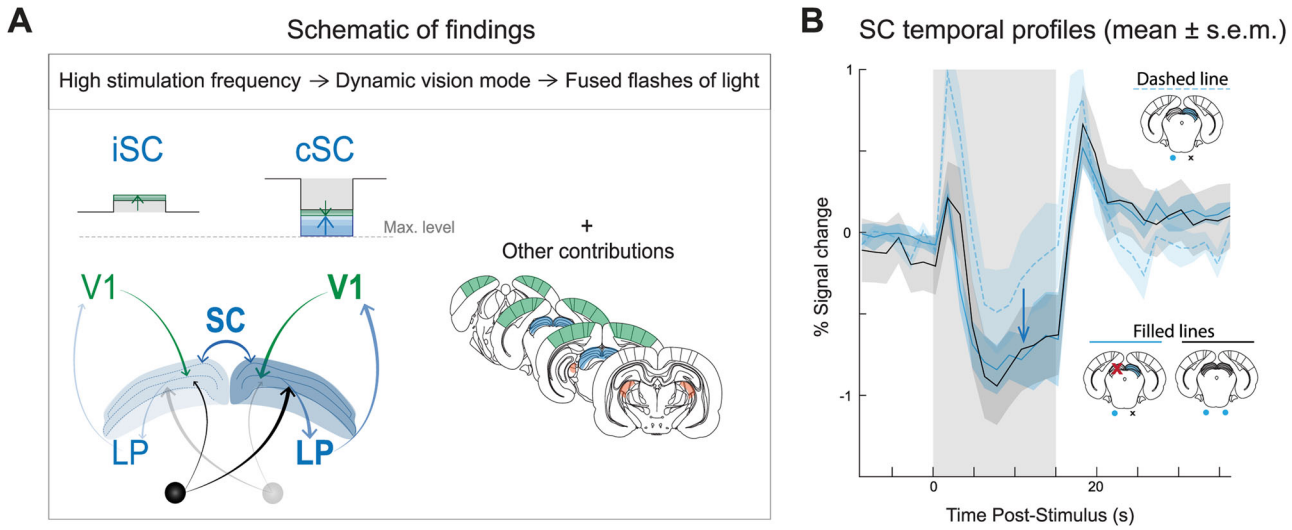

Fig. 4 | Proposed interactions during the dynamic vision mode. A The findings described in this study suggest a cortical amplification effect (represented in green) and a push-pull interaction between SC's (represented in blue). This study focused on the effects of corticotectal and tectotectal feedback and therefore, contributions from other visual pathway structures cannot be discarded. We propose that the high frequency stimulus (in grey), combined with the cortical potentiation effects (in green), induces maximal cSC suppression (and, consequently, maximal negative fMRI response) which is opposed by the positive iSC responses since mostly one eye is receiving such visual stimulus. Following this prediction, the cSC responses upon monocular stimulation would become similar to the negative SC responses upon binocular stimulation (where both SC's would be maximally suppressed by the visual stimuli hitting both eyes combined with cortical potentiation) when the iSC is further silenced; **B** When comparing the responses for the two stimulation regimes in healthy animals, the amplitude of the monocular responses (blue dashed line) showed less negative amplitude during the ON period than the binocular responses (black filled line). When the iSC was silenced (blue filled line) the monocular responses became identical to the binocular responses, supporting the counter-balancing role of the iSC on the negative cSC responses. cSC contralateral superior colliculus, iSC ipsilateral superior colliculus.

Our findings suggest that, unlike its static vision mode counterpart, the dynamic vision mode evokes a marked push-pull interaction between the contralateral and ipsilateral SCs. As the system enters into the dynamic vision mode, and the cSC activity is suppressed, the iSC engages in relatively strong activation. In other words, while the cSC 'pushes' downward towards deactivation, the iSC 'pulls' the signal upwards towards a less deactivated state. Indeed, when the iSC was lesioned, the iSC 'pulling' was abolished, generating a dramatically stronger deactivation in the cSC (Fig. 3D–F). In addition, the positive iSC response was quite independent of corticotectal feedback (as evident from the V1-lesioned group responses seen in Fig. 3A–C) unlike its cSC counterpart (which is affected by corticotectal feedback), suggesting that the main push-pull interaction occurs at the tectotectal level, with little interference from other areas, potentially hinting at more complex tectotectal interactions than previously considered.

Based on these findings we can now propose a tentative mechanism for the different interactions occurring during the dynamic vision mode (Fig. 4A). The activity in the SC is strongly suppressed when entering the dynamic vision mode and cortical feedback potentiates the suppression towards a maximal level (represented in green in Fig. 4A): in binocular stimulation, the two SCs are suppressed to this level, likely signalling a bilateral agreement about the input. If, however the stimulation is monocular, the iSC activates, likely through tectotectal feedback from the cSC, exerting a 'pull' effect on the cSC, leading to a less suppressed state, potentially either creating a diminished threshold for detecting novel stimuli in the eye that is seeing continuous light, or signalling that the two eyes are not in agreement.

Given this proposed mechanism, we can make two simple predictions: (1) cSC responses upon monocular stimulation should present less negative responses compared to the (two) SC signals upon binocular stimulation (because the pull element is not present in the latter, both SC's are simultaneously 'cSC' and 'iSC' in a sense); and (2) lesioning the iSC should prevent the tectotecal 'pull' element exerted on the cSC in monocular stimulation, thereby allowing the cSC's signal to reach the level it would potentially attain upon binocular stimulation in the dynamic vision mode. To test these predictions, we measured the SC signals under all these scenarios (Fig. 4B). Indeed, our predictions are observed in these experiments. SC signals are more negative for binocular stimulation compared to monocular stimulation, and when we lesioned only iSC and performed monocular stimulation, the cSC signals became more negative, reaching the binocular stimulation levels (Fig. 4B, filled lines). We note in passing that our study focuses on the corticotectal and tectotectal feedback, and therefore contributions from other structures within the visual pathway, such as lateral posterior thalamic nucleus (LP), LGN or higher order visual areas, cannot be ruled out. Nevertheless, our findings point to a major tectotectal push-pull effect that originates within the tectum.

The SC is part of the tectum which, additionally, encompasses two posterior inferior colliculi (ICs). The IC is a major midbrain auditory integration centre and as the SC and the IC are both tectal multimodal structures, they are indeed connected. For example, the IC coordinates with the SC in orienting the gaze toward or away from visual and auditory stimuli[5] and an inferior-superior colliculus circuit providing key visual spatial attention signals has been reported[36]. Interestingly, a push-pull like mechanism[37–39] - stronger contralateral excitation and ipsilateral inhibition - occurs between the two ICs, playing important roles in resolving sound intensity disparities in the context of sound localisation and lateralisation[37]. While behaviour was not performed in this study, the IC analogue of push-pull interactions is associated with monaural and binaural sound integration, and this could hint that the SC push-pull interactions observed here may either facilitate a compensatory mechanism to balance visual processing states and/or serve as part of a more complex tectal network involved in visual localisation, lateralised motion encoding, along with optical flow processing. Although this type of computation is usually associated with cortical areas[40] in higher-order mammals, the rodent SC is more prominent for visual processing[14,41]. Therefore, in lower-order animals, the involvement of SC in such visual localisation processing is plausible. Future studies could test these hypotheses by disrupting the SC push-pull balance through transient modulation methods, such as such as optogenetics[42–45] or pharmacology[46,47], and assess behavioural responses, or by examining animals with altered visual experience to determine how changes in ocular dominance influence FFF thresholds.

The push-pull mechanism was clearly observed in the dynamic vision mode, but the static vision mode likely operates within a different interaction, as proposed in Supplementary Fig. 7 based on the findings reported in Supplementary Fig. 5. Maximal positive responses in the cSC arise from a combination of the contralateral activity elicited by the visual stimulus (represented in grey in Supplementary Fig. 7A), cortical potentiation (represented in green in Fig. S7A) and an intertectal boosting effect (represented in blue in Supplementary Fig. 7A), as both SCs present responses of the same polarity. Therefore, we hypothesise that this maximal activation regime would be reached both in healthy monocular cSC responses and in healthy binocular positive responses. Consequently, silencing iSC inputs would then result in less positive monocular cSC responses. Indeed, the amplitude of healthy responses for both stimulation regimes (monocular and binocular) appeared similar, in-line with our hypothesis (Supplementary Fig. 7B), and a general decrease in positive amplitude of responses was seen in the monocular iSC-lesioned regime.

The distinct mechanisms proposed for the two vision modes (Fig. 4A and Supplementary Fig. 7A) suggest a higher degree of complexity at the commissural level between the two SCs than previously thought. Although the modulation of SC activity appears to go in a similar direction for both vision modes due to ipsilateral tectal inputs, there is an important distinction between the two: in the static vision mode the intertectal communication appears to have an additive effect, while in the dynamic vision mode, there is an opposing effect. Although intertectal SC connections have been mostly assumed to be inhibitory, reports of equal glutamatergic and GABAergic intertectal connections[30] with similar topographic distribution in the cat support the idea that the tectotectal pathway may consist of two distinct functional components. Moreover, another study performed in cats[48] revealed specific spatial distributions of commissural excitation and inhibition, which were associated with saccadic eye movements: while excitation was recorded between the medial-medial or lateral-lateral parts of both SCs; commissural inhibition was observed between the medial sub-region of one SC and lateral sub-region of the opposite SC. Our work reveals that the suggested complexity of the tectotectal pathway also exists in the rat animal model even for simple visual stimuli that target the entirerity of the animal's field of view and where saccades are not expected to occur (therefore dissociating this effect from saccade occurrence).

Ipsilateral tectal inputs could lead to an overall increase in cSC neural activity through two distinct mechanisms: (i) decreased inhibitory cSC activity or (ii) increased excitatory cSC activity. In the first scenario, intertectal inhibitory inputs might target inhibitory neurons within the cSC, effectively silencing these cells and, consequently, disinhibiting their excitatory projections. In the second scenario, intertectal excitatory inputs could directly activate excitatory cSC neurons, thereby enhancing cSC neural activity. Further studies integrating behavioural assessments and/or transient manipulation of specific SC cell types (for example using optogenetics) are needed to determine which mechanism predominates in each vision mode, or whether both are engaged simultaneously with varying degrees of influence. These dynamic intertectal interactions, potentially involving distinct neural circuits due to the different spatial distribution of positive and negative SC signals, may play a crucial role in shaping appropriate behavioural responses to different visual stimuli (e.g., differentiating between slow- and fast-approaching objects)[30].

Interestingly, negative fMRI cSC responses were predominantly observed in more medial regions of the rat SC, areas associated with defensive behaviours as they correspond to the upper visual field - from where aerial predators typically approach. Given that the visual stimulus in this study covered the entire field of view, interpreting the behavioural relevance of the distinct spatial distributions of positive and negative fMRI tectal responses is complex. Nevertheless, it is notable that contralateral negative responses during the dynamic vision mode appear more localised in regions linked to defensive behaviours. Future electrophysiological studies are required to further elucidate the specific neuronal mechanisms behind the distinct signal modulation patterns observed when shifting from the static to the dynamic vision mode.

The above discussion has focused mostly on the observed ON period modulations of the SC responses; however, another important finding of our work is that fMRI signals contain "fine structure" that allows for the detection of response dynamics, including onset and offset signals (associated with novelty detection). It is interesting to notice how cortical gain did not play a significant role on offset responses (evidenced by the difference maps in Fig. 3C), while tectotectal input mostly affected these signals (evidenced by the difference maps in Fig. 3F). While this suggests that the two signal peaks may originate from different sources - a question that could be addressed in future studies using electrophysiological approaches - an important factor to consider is the temporal resolution of the fMRI BOLD signals acquired in this study (repetition time = 1.5 s), which may be insufficient to fully resolve the onset and offset peaks. Future research combining ultrafast MRI techniques[49–52] with high temporal resolution methods, such as two-photon[53,54] or calcium imaging[55–58], to capture activity at the level of specific cell types, will be crucial for a deeper understanding of the novel push-pull interaction reported here. It is plausible that, although both signal peaks correspond to novelty-related events, they reflect distinct processes: the onset peak likely marks the arrival of light to the SC, potentially dominated by retinal inputs, whereas the offset peak may reflect the absence of light, integrating effects from both feedback and intra-SC mechanisms. To further dissect these dynamics, fMRI experiments employing an inverted stimulation paradigm - where the resting condition involves constant light and the stimulation consists of light absence - could help elucidate how 'light arrival' influences onset and offset signals. Additionally, a limitation of fMRI when analysing such 'fine structure' is the potential conflation of multiple neural processes within regions lacking clear temporal segregation. For example, post-stimulus undershoots or overshoots could be mistaken for offset responses in general linear model (GLM) analyses. Careful interpretation is needed in such cases. However, this type of signal decomposition can be highly informative, particularly when validated with complementary electrophysiological data, as demonstrated in our recent work[15].

While tectotectal feedback seems to have a significant influence, the current data cannot rule out contribution from non-crossing RGCs. However, the fact that, in the rodent visual system, approximately 95–97% of retinal ganglion cells (RGCs) cross at the optic chiasm, while the remaining 3-5% project to the iSC, supports the idea that, if anything, the contribution from non-crossing RGCs would be minimal. Still, it is important to discuss in more detail the observed iSC responses (measured in both vision modes) along with the potential contribution from non-crossing RGCs. Although rodents have reduced binocular field and limited depth perception, studies[59,60] have revealed binocular responses in the rodent SC, suggesting that binocular vision plays important roles in, for example, behaviours such as prey capture, where rodents require vision to see and approach the prey animals[61]. In such studies, iSC responses were investigated through electrophysiological recordings, which did not prevent inputs from the contralateral SC (which was not silenced) to reach the iSC. Therefore, which components of ipsilateral activity resulted from the 3–5% non-crossing RGCs or from the cSC remain unclear. In addition, in a previous work employing binocular stimulation[15] a strong modulation of the SC activity, which was dependent on the used stimulation frequency, was observed. Given that the superficial layers of the SC are predominantly driven by retinal inputs, it seems counterintuitive that identical visual stimuli would result in such distinct activity between the contralateral and ipsilateral SCs, as one might expect similar RGC inputs to produce comparable responses in both hemispheres. Nevertheless, in the present work, results can only inform on the effects of the iSC on the cSC and not the other way around and therefore, we cannot rule out that iSC activity might result, in part, from non-crossing RGCs.

Our findings, along with previous work[15], suggest cortical facilitation/amplification of SC activity during both static and dynamic vision modes, yet its role in modulating FFF threshold remains uncertain. While facilitation was observed for extreme frequencies within both vision modes, cortical influence near the FFF threshold is less pronounced[15] suggesting that

cortical feedback primarily acts as a gain mechanism rather than directly modulating this threshold. Existing literature[62,63] supports the notion that the SC functions as a high-pass filter, potentially influencing FFF thresholds via inhibitory mechanisms. Here, we hypothesize that specific intra-SC circuits, particularly involving GABAergic neurons, may regulate suppression states at high stimulation frequencies. In fact, the SC visual layers comprise 50% GABAergic neurons[13] and investigating which cell types are mostly affected (and why) when changing the stimulation frequency is key to target these specific cells for activation/silencing and study potential FFF threshold modulations. Future studies harnessing more refined transient brain modulation approaches, such as optogenetics[42–45] or pharmacological[46,47] studies, offer a controlled approach to study the cortical effect in SC response regulation and could provide further insight into SC's role in perceptual limits. Finally, behavioural studies employing such transient modulation of V1 or SC visual layers will be key in testing these hypotheses.

An additional important point of discussion is the applicability of the findings from this study to higher-order species, specifically regarding the relevance of the extrageniculate pathway in visual perception. While the SC is an evolutionarily conserved structure[64], the mammalian visual pathway has undergone species-specific adaptations to support distinct visual behaviours[3]. In all mammals, the visual system operates through two parallel pathways - the geniculate and extrageniculate pathways. Several studies have highlighted a more central role for the SC (a key component of the extrageniculate pathway) in rodent vision, emphasizing its involvement in reflexive visual behaviours. In contrast, this role is largely assumed by the geniculate pathway and the visual cortex in higher-order species[14,41,65]. However, the greater emphasis placed on the geniculate pathway and cortical mechanisms in higher-order mammals does not exclude the contribution of the extrageniculate pathway and its subcortical structures. For example, evidence suggests that the pulvinar thalamic nucleus - a major projection target of the SC (referred to as LP in rodents) - is involved in the cognitive processing of optical illusions, such as the continuity illusion, that occurs during the dynamic vision mode, in humans[66]. Furthermore, the pulvinar and other non-geniculate routes play critical roles in conditions like blindsight, where individuals with cortical blindness retain the ability to detect, localize, and even discriminate visual stimuli without conscious awareness[67]. These findings point to a potentially greater relevance of the extrageniculate pathway in higher-order species than traditionally considered. Nonetheless, the extent to which the findings from this work apply to higher-order species remains unknown, and future studies are needed to explore this topic in greater detail.

It is interesting to point out that the whole-system view offered by fMRI also allows the investigation of other subcortical areas with respect to static/dynamic vision modes. For instance, LGN signals (shown in Supplementary Figs. 4, 6 and 8), although positive throughout the different stimulation paradigms, also appear modulated in the different vision modes with decreased amplitude seen at high stimulation frequencies (Supplementary Fig. 8). This structure receives similar inputs as the SC with the additional SC inputs themselves originating from stellate cells - which can be excitatory and inhibitory - and from horizontal cells - known to be inhibitory[3,68]. Upon V1 lesioning, while in the static vision mode LGN responses do not change (Supplementary Fig. 8, orange lines), they do show an increased signal amplitude in the dynamic vision mode (Supplementary Fig. 8, black lines). Interestingly, LGN signals upon V1 lesions in the dynamic vision mode become very similar to the healthy LGN responses in the static vision mode reaching ~0.7% signal change (Supplementary Fig. 8, black and orange filled lines). This suggests that the observed LGN modulation is not likely to occur within LGN itself but probably arises from cortical feedback and/or SC inputs, both of these regions within neural suppression states during the dynamic vision mode. Further experiments silencing the contralateral SC or the LGN itself will give additional insights into the SC-LGN pathway in the different vision modes.

Finally, several methodological aspects and limitations merit further discussion. In the current study, we resorted to brain lesions targeting key structures of the visual pathway to selectively reduce tectal feedback connections (the injection effects were studied in Supplementary Fig. 9 upon saline injection in the V1).

One disadvantage of using brain lesions for silencing a specific region is the variability of the lesions performed in different animals. When targeting small brain regions or cell populations, indeed, brain lesioning is not advisable and other more specific techniques, such as optogenetics/chemogenetics, should be used for a more precise effect. However, in our study, the desired effect - namely, a successful silencing of signals from the majority of the targeted region (which were large enough to lesion effectively) - was achieved. We note that the specific coverage of each lesion or the inflammation/swelling still present after a certain time interval had subtle variations between animals. This can lead to a small degree of variability in the BOLD fMRI results, but as seen at the top of Supplementary Fig. 2, those were relatively small, in part due to our specific targeting of the structure to lesion according to anatomical MRI scans performed a-priori for each rat, and also our ability to confirm lesion locations with post lesioning MRI anatomical scanning.

Furthermore, brain lesioning is a permanent manipulation where the affected region cannot regain function. This can lead to neural plasticity events that may already take place during the period between the lesion and data acquisition. In the current study, lesioned animals were allowed to recover for 7-9 days before being imaged. This time interval was chosen to allow for (i) the animal's recovery, (ii) for the lesions to produce their effects, and (iii) to minimise inflammation (which on its own could be a confounding effect). Although at least a partial recovery of SC's normal activity is expected according to previous studies[69], this recovery process probably also involves some degree of plastic changes in other areas and connections, in an attempt to compensate for the initial lesion. Larger plasticity events, however, are thought to take place across longer time frames[69]. Importantly, our results are qualitatively comparable to Goodale's work[18], which included collicular and cortical lesions in the rat during bipolar electrode recordings and where activity was recorded immediately before and after the lesion. This similarity points at a relatively small contribution of plasticity in our measurements. In addition, some slight systemic effects in the lesion models cannot be completely ruled out (Supplementary Fig. 9), but, if present, their impact on the conclusions of this work would be minimal due to the much smaller effect compared to the lesion consequences.

Also, spontaneous neural activity unrelated to the visual stimulus is unlikely to have significantly contaminated our results as, for every animal, the time profiles are averaged across multiple runs, which were measured at different time points during entire sessions that lasted ~3.5 h. In such cases, varying baseline spontaneous neural activity (which for sure takes place) will likely be averaged out, and then when averaged across different animals such effects would be expected to be further mitigated.

Finally, the use of anaesthesia when studying functional processes may affect the interplay between bottom-up and top-down pathways differently depending on the anaesthetic used. Particularly for the SC, it has been shown that under the effect of urethane[18,70] or isoflurane[21,71], the corticotectal connections, top-down inputs to the SC, are more affected than the bottom-up retinal inputs or the intertectal interactions, and can sometimes even be completely masked[19]. In the present study, animals were lightly sedated with medetomidine, an α2 agonist[72], whose effects have been shown to be small when comparing baseline neural activity to awake[73]. A good agreement between SC responses under medetomidine sedation and behavioural measurements has been observed[15] along with similarities to studies in awake mice[74]. Furthermore, studies in rats, with a similar medetomidine protocol as the one used in this work, have reported functional connectivity partially attributed to wakefulness[75]. Therefore, although we cannot rule out possible changes in the visual pathway during medetomidine sedation, taking these favourable comparisons into account, we believe that the use of medetomidine anaesthesia did not strongly affect our results.

In conclusion, we report a push-pull interaction between the two SCs during the dynamic vision mode where individual flashes are perceived as a continuous light stimulus. While cSC responses were suppressed by the

visual stimulus, positive responses in the iSC pulled cSC into a less deactivated state, and these interactions were observed independently of cortical lesions. Further silencing the iSC responses led to stronger negative fMRI cSC responses identical to the healthy binocular ones observed during the dynamic vision mode. The proposed interactions occurring between the two SCs were different for low and high stimulation frequencies suggesting a complex SC intertectal interplay that is modulated by stimulation frequency. Finally, the distinct spatial segregation of positive and negative fMRI SC responses suggests different tectotectal mechanisms in the static vs. the dynamic vision mode, each probably associated with activation of different commissural connections. Our findings suggest a higher complexity of the tectotectal pathway than a simple reciprocal inhibitory effect.

Methods

All animal care and experimental procedures were carried out according to the European Directive 2010/63 and pre-approved by the competent authorities, namely, the Champalimaud Animal Welfare Body and the Portuguese Direcção-Geral de Alimentação e Veterinária (DGAV).

In this study, $n = 27$ adult Long-Evans rats ($n = 18$ females) were used. The animals had *ad libitum* access to food and water and were kept under a normal 12 h/12 h light/dark cycle. Rats were randomly split into three groups (Fig. 1A): The fMRI healthy group consisted of 7 rats ($n = 4$ females): 14.9 ± 3.9 weeks old, weighing 349.1 ± 87.5 g on average. The fMRI V1-lesioned group consisted of 8 rats ($n = 3$ females): 16.8 ± 0.9 weeks old, weighing 357.5 ± 57.9 g on average. The fMRI V1+iSC-lesioned group consisted of 7 rats ($n = 6$ females): 24.7 ± 7.7 weeks old, weighing 306.3 ± 31.6 g on average. A fourth group where the iSC was lesioned consisted of 5 rats (n = 5 females): 22.8 ± 3.2 weeks old, weighing 400.6 ± 24.1 g on average.

Ibotenic acid lesions and perfusion

Animals were injected with an ibotenic acid (Abcam, Romania) solution (excitotoxic agent, 1 mg/100 µL) either bilaterally in the V1 ($n = 8$), unilaterally in the iSC ($n = 5$), or simultaneously bilaterally in the V1 and the iSC ($n = 7$), to investigate the effect of cortical or tectal feedback projections in the cSC activity. Ibotenic acid is an excitotoxin that damages cells by causing a large influx of calcium into the cell thus creating an excessive release of glutamate and activation of excitatory plasma membrane receptors[76]. Due to its affinity with NMDA glutamate receptors, it mainly targets excitatory neurons[77,78] which leads to a lesioned area where a diffuse border of sparser cell density and/or with no intact neurons can be identified[79]. Therefore, lesions performed with ibotenic acid are expected to predominantly target cholinergic neurons, while leaving the vasculature and passing fibres on that region intact[79,80]. Apart from the tissue mechanical damage induced due to the necessary use of a glass pipette, lesions performed with ibotenic acid are not expected to dramatically affect tissue integrity immediately[79,81]. This was confirmed with histological images (Supplementary Fig. 3) when perfusion was done around the scanning time post-lesion (7–9 days). However, tissue integrity appears increasingly compromised over time which can be observed in the histology images from Fig. 1A where perfusion was performed 3 months post-lesion.

The acid was injected using a Nanojet II (Drummond Scientific Company). Animals were anaesthetised with isoflurane (anaesthesia induced at 5% concentration and maintenance below 3% in medical air), and a scalpel incision was made along the midline of the skull, the skin retracted and the soft tissue cleaned from the skull with blunt forceps.

Coordinates for the craniotomies and number of injections required were determined for each individual animal based on T_2-weighted anatomical images acquired before the surgery. Injections were made in a maximum of 5 different Anterior-Posterior (AP) coordinates, with 1 injection site for the first AP coordinate (2 pulses of injection) and 2 for the following ones (4 pulses of injection each), for full coverage of the V1. For full coverage of the SC, 3 injections were performed in different AP coordinates, each with 3 medio-lateral (ML) injection sites (vertical insertion, 2 pulses of injection each). For the second and third AP coordinate an extra injection was performed at a 20° angle with the vertical (2 pulses of injection). Each injection pulse was administered at a rate of 23 nL/s, waiting 2–3 s between pulses and each pulse consisted of 32 nL for the V1 and 23 nL for the SC injections. The waiting time before removing the injection pipette after the last pulse was 10 min. The craniotomies were then covered with Kwik-Cast™ (World Precision Instruments, USA) and the scalp was sutured. Before the animals recovered from surgery, they were injected subcutaneously with 5 mg/Kg body weight of carprofen (Rimadyl ®, Zoetis, U.S.A). Following surgery, the animals were allowed to recover for 7-9 days to avoid MRI acquisition artefacts due to potential inflammation.

For post-mortem confirmation of the lesions (~3 months after MRI scanning), the animals were overdosed with pentobarbital (100 mg/kg of body weight, intraperitoneal injection) and perfused transcardially with a solution of 4% PFA for a period of 12–24 h before slicing for further microscopy imaging (Fig. 1A).

Visual set-up and paradigm for fMRI acquisitions

The flashing stimulation was performed at two frequencies frequency (1 Hz and 25 Hz) known to induce the static and dynamic vision modes, respectively[15], and the flash duration was set to 10 ms. The stimulation paradigm consisted of a 15 s stimulation period interleaved with 45 s rest periods (Fig. 1B) and this cycle was repeated 6 times in each MRI acquisition run.

The stimulated eye of the animal was hydrated at the start of acquisition with ophthalmic gel (Vidisic gel Bausch + Lomb, Portugal) and the tip of an optic fibre connected to a blue LED ($\lambda = 470$ nm and $I = 8.1 \times 10^{-1}$ W/m^2) was placed horizontally in front of it, spaced up to 1 cm from the animal (Fig. 1C). To achieve a successful monocular stimulation regime, the other eye was covered with an opaque gel (Bepanthen augen und nasensalbe) and a piece of black polyurethane-coated nylon fabric to avoid any light from entering. The blue LED was connected to an Arduino MEGA2560 receiving triggers from the MRI scanner and was used to generate square pulses of light. Given the position of the optic fibre relative to the stimulated eye and the fact that the blue light reflected inside the MRI bore, the entire field of view of the animal was considered to be stimulated.

Animal preparation for fMRI acquisition

Anaesthesia was induced with 5% isoflurane (Vetflurane, Virbac, France) in medical air for 2 min, and the animals were then weighed and transferred to the MRI bed. Sedation began through an injection of a subcutaneous bolus (0.05 mg/kg) of medetomidine solution (1:10 dilution in saline of 1 mg/ml medetomidine solution—Vetpharma Animal Health, S.L., Spain), 5 min after the initial isoflurane induction. Isoflurane was gradually reduced to 0% during the following 10 min, whereupon a constant infusion of medetomidine (0.1 mg/kg/h) was initiated via a syringe pump (GenieTouch, Kent Scientific, Torrington, Connecticut, USA). For the rest of the MRI session, animals remained only under continuous medetomidine sedation. To ensure sufficient isoflurane washout, the fMRI acquisitions were started 30 min after medetomidine bolus injection. In the end of each MRI session, the medetomidine sedation was reverted by injecting an equal volume of the initial bolus of a 5 mg/ml solution of atipamezole hydrochloride (Vetpharma Animal Health, S.L., Spain) diluted 1:10 in saline. During the fMRI experiments, animals breathed a mixture of 95% oxygen and 5% medical air.

The animal's temperature was constantly monitored with a rectal temperature optic fibre probe (SA Instruments, Inc., Stony Brook, New York, USA) and was kept at 36.5 ± 1.0 °C via water circulating through a heat pad placed underneath the animal. The respiratory rate was measured using a pillow sensor (SA Instruments Inc., Stony Brook, USA) and was kept at 89.1 ± 17.7 breaths/min for the entire fMRI session.

MRI acquisitions

The experiments were conducted on a 9.4 T Bruker Biospec MRI scanner (Bruker, Karlsruhe, Germany) equipped with an AVANCE III HD console, a gradient unit capable of producing pulsed field gradients of up to 660 mT/m isotropically with a 120 µs rise time, and ParaVision®6.0.1 software. An

86 mm quadrature coil was used for radiofrequency transmission and a 4-element array cryoprobe[82] (Bruker, Fallanden, Switzerland) was used for signal reception.

For correct slice placement along the visual pathway, an anatomical T_2-weighted Rapid Acquisition with Refocused Echoes (RARE) sequence was first acquired (TR/TE = 1600 / 36 ms, RARE factor = 8, Echo spacing = 9 ms; Averages = 3; FOV = 18 × 16 mm^2, in-plane resolution = 168 × 150 μm^2, slice thickness = 800 μm, t_{acq} = 1 min 3 s). In a subset of animals, the anatomical acquisition was acquired with slightly different parameters: TR/TE = 3000 / 40 ms, RARE factor = 12, Echo spacing = 6 ms; Averages = 2; FOV = 18 × 16 mm^2, in-plane resolution = 168 × 150 μm^2, slice thickness = 800 μm, t_{acq} = 48 s.

The fMRI scans were acquired using a Spin-Echo Echo-Planar Imaging (SE-EPI) sequence (TR/TE = 1500 / 40 ms, Partial Fourier Factor (pFT) = 1.5, FOV = 18 × 16.1 mm^2, in-plane resolution = 269 × 268 μm^2, slice thickness = 1.5 mm, 8 slices, t_{acq} = 6 min 50 s).

fMRI data analysis

The data was analysed using MATLAB (The Mathworks, Natick, MA, USA, v2016a and v2018b).

A general linear model (GLM) analysis was conducted voxel-wise along with a region of interest (ROI) analysis based on anatomy to gain insight into the temporal dynamics of activation profiles.

GLM Analysis: Pre-processing steps included manual outlier removal through a spline interpolation taking the entire acquisition run (<0.0005% of the data were identified as outliers), slice-timing correction (using a sinc-interpolation) followed by head motion correction (using a mutual information algorithm). Data was then co-registered to the T_2-weighted anatomical images, normalised to a reference animal and smoothed using a 3D Gaussian isotropic kernel with full width half-maximum of 0.268 mm. A double gamma hemodynamic response function (HRF) peaking at 0.2 s was convolved with the stimulation paradigm to obtain an experimental regressor of the design matrix peaking at 1.75 s (around the time fMRI temporal profiles peaked).

From the dynamic vision mode contralateral time profiles, it became apparent that the cSC responses were multi-periodic (c.f. Results) and could be decomposed into three distinct periods: onset, ON and offset. Therefore, the three periods were used in a second GLM as 3 independent regressors after being convolved with a similar HRF peaking at 0.2 s. The onset regressor was designed to peak 1.75 s after the stimulation started; the ON regressor peaked 6.25 s after stimulation started; and the offset regressor peaked 3.25 s after the stimulation finished.

A fixed-effects group analysis was run independently for each group and for the difference between two groups. Resulting t-value maps were thresholded with $p < 0.005$ and a minimum cluster size of 10 voxels, and were cluster-FDR corrected at $p < 0.005$, both when analysing each group and the difference between groups.

ROI Analysis: The 6th Edition of Paxinos & Franklin's rat brain atlas[83] was used for manual ROI delineation. The individual normalised fMRI runs were detrended with a 2nd degree polynomial fit to the first resting period and the final 10 s of the subsequent resting periods to remove low-frequency trends. The detrended data were then converted into percent signal change relative to baseline. For each run, the six individual cycles were separated and the averaged response was calculated within each ROI (along with the standard error of the mean), first at the animal level and afterward at the group level. Average signals per animal were used for statistical analysis.

Temporal signal-to-noise ratio (tSNR) calculation: The tSNR was calculated to investigate the effect of the lesions in the ROI quantifications (Supplementary Fig. 1B). The ROIs drawn for the cSC and contralateral LGN during the ROI analysis were used to calculate tSRN values. For each animal, the voxelwise mean and signal standard deviation during rest periods was calculated. The tSNR values were then obtained by dividing the mean signal by the standard deviation and the average values for each animal were calculated. Finally, for each group, the animal tSNRs for each ROI were averaged and the standard error of the mean was calculated.

Reporting summary

Further information on research design is available in the Nature Portfolio Reporting Summary linked to this article.

Data availability

The source data that supports the findings described in this paper is available as a figshare repository (https://doi.org/10.6084/m9.figshare.28555010[84]). The source data behind the graphs in the figures can be found in Supplementary Data 1. Other data can be made available upon reasonable request to the corresponding author.

Code availability

All the code used to generate the results in this study can be made available upon reasonable request.

Received: 18 May 2024; Accepted: 11 April 2025;
Published online: 22 April 2025

References

1. Isa, T., Marquez-Legorreta, E., Grillner, S. & Scott, E. K. The tectum/superior colliculus as the vertebrate solution for spatial sensory integration and action. *Curr. Biol.* **31**, R741–R762 (2021).
2. A. Wilks, T., R. Harvey, A. & Rodger, J. Seeing with Two Eyes: Integration of Binocular Retinal Projections in the Brain. in *Functional Brain Mapping and the Endeavor to Understand the Working Brain* 227–250 (InTech). https://doi.org/10.5772/56491, (2013).
3. Cang, J., Savier, E., Barchini, J. & Liu, X. Visual function, organization, and development of the mouse superior colliculus. *Annu Rev. Vis. Sci.* **4**, 239–262 (2018).
4. Wheatcroft, T., Saleem, A. B. & Solomon, S. G. Functional organisation of the mouse superior colliculus. *Front. Neural Circuits* **16**, 792959 (2022).
5. King, A. J. The superior colliculus. *Curr. Biol.* **14**, R335–R338 (2004).
6. Binns, K. E. & Salt, T. E. Excitatory amino acid receptors modulate habituation of the response to visual stimulation in the cat superior colliculus. *Vis. Neurosci.* **12**, 563–571 (1995).
7. Phongphanphanee, P. et al. Distinct local circuit properties of the superficial and intermediate layers of the rodent superior colliculus. *Eur. J. Neurosci.* **40**, 2329–2343 (2014).
8. Dean, P., Redgrave, P. & Westby, G. W. M. Event or emergency? Two response systems in the mammalian superior colliculus. *Trends Neurosci.* **12**, 137–147 (1989).
9. Mayo, J. P. & Sommer, M. A. Neuronal adaptation caused by sequential visual stimulation in the frontal eye field. *J. Neurophysiol.* **100**, 1923–1935 (2008).
10. Platt, B. & Withington, D. J. Response habituation in the superficial layers of the guinea-pig superior colliculus in vitro. *Neurosci. Lett.* **221**, 153–156 (1997).
11. Dyer, R. S. & Annau, Z. Flash evoked potentials from rat superior colliculus. *Pharm. Biochem. Behav.* **6**, 453–459 (1977).
12. Oyster, C. W. & Takahashi, E. S. Responses of rabbit superior colliculus neurons to repeated visual stimuli. *J. Neurophysiol.* **38**, 301–312 (1975).
13. Mize, R. R. The organization of GABAergic neurons in the mammalian superior colliculus. *Prog. Brain Res.* **90**, 219–248 (1992).
14. Wang, L., Sarnaik, R., Rangarajan, K., Liu, X. & Cang, J. Visual receptive field properties of neurons in the superficial superior colliculus of the mouse. *J. Neurosci.* **30**, 16573–16584 (2010).
15. Gil, R., Valente, M. & Shemesh, N. Rat superior colliculus encodes the transition between static and dynamic vision modes. *Nat. Commun.* **15**, 849 (2024).
16. Yang, S. et al. The electroretinogram of Mongolian gerbil (Meriones unguiculatus): comparison to mouse. *Neurosci. Lett.* **589**, 7–12 (2015).

17. Lisney, T. J., Ekesten, B., Tauson, R., Håstad, O. & Ödeen, A. Using electroretinograms to assess flicker fusion frequency in domestic hens Gallus gallus domesticus. *Vis. Res.* **62**, 125–133 (2012).
18. Goodale, M. A. Cortico-tectal and intertectal modulation of visual responses in the rat's superior colliculus. *Exp. Brain Res.* **17**, 75–86 (1972).
19. Zhao, X., Liu, M. & Cang, J. Visual cortex modulates the magnitude but not the selectivity of looming-evoked responses in the superior colliculus of awake mice. *Neuron* **84**, 202–213 (2014).
20. Tamai, M. & Tetsuro, O. Interaction between cortico-tectal and retino-tectal inputs as revealed by analysis of field potentials of the cat's superior colliculus. *Tohoku J. Exp. Med*. **107**, 127–142 (1972).
21. Stitt, I., Galindo-Leon, E., Pieper, F., Engler, G. & Engel, A. K. Laminar profile of visual response properties in ferret superior colliculus. *J. Neurophysiol.* **110**, 1333–1345 (2013).
22. Bereshpolova, Y., Stoelzel, C. R., Gusev, A. G., Bezdudnaya, T. & Swadlow, H. A. The impact of a corticotectal impulse on the awake superior colliculus. *J. Neurosci.* **26**, 2250–2259 (2006).
23. Rizzolatti, G., Tradardi, V. & Camarda, R. Unit responses to visual stimuli in the cat's superior colliculus after removal of the visual cortex. *Brain Res.* **24**, 336–339 (1970).
24. Rosenquist, A. C. & Palmer, L. A. Visual receptive field properties of cells of the superior colliculus after cortical lesions in the cat. *Exp. Neurol.* **33**, 629–652 (1971).
25. Ogasawara, K., Mchaffie, J. G. & Stein, B. E. Two visual corticotectal systems in cat. *J. Neurophysiol.* **52**, 1226–1245 (1984).
26. Takahashi, M., Sugiuchi, Y., Izawa, Y. & Shinoda, Y. Commissural excitation and inhibition by the superior colliculus in tectoreticular neurons projecting to omnipause neuron and inhibitory burst neuron regions. *J. Neurophysiol.* **94**, 1707–1726 (2005).
27. Hoffmann, K. P. & Straschill, M. Influences of cortico-tectal and intertectal connections on visual responses in the cat's superior colliculus. *Exp. Brain Res*. **12**, 120–131 (1971).
28. Robert, F. & Cuénod, M. Electrophysiology of the Intertectal commissures in the pigeon II. Inhibitory interaction. *Exp. Brain Res.* **9**, 123–136 (1969).
29. Sprague, J. M. Interaction of cortex and superior colliculus in mediation of visually guided behavior in the cat. *Science***153**, 1544–1547 (1966).
30. Olivier, E., Corvisier, J., Pauluis, Q. & Hardy, O. Evidence for glutamatergic tectotectal neurons in the cat superior colliculus: A comparison with GABAergic tectotectal neurons. *Eur. J. Neurosci.* **12**, 2354–2366 (2000).
31. Mascetti, G. G. & Arriagada, J. R. Tectotectal interactions through the commissure of the superior colliculi: an electrophysiological study. *Exp. Neurol.* **71**, 122–133 (1981).
32. Pawela, C. P. et al. Modeling of region-specific fMRI BOLD neurovascular response functions in rat brain reveals residual differences that correlate with the differences in regional evoked potentials. *Neuroimage* **41**, 525–534 (2008).
33. Bailey, C. J. et al. Analysis of time and space invariance of BOLD responses in the rat visual system. *Cereb. Cortex* **23**, 210–222 (2013).
34. Zhang, Q. et al. High-frequency neuronal signal better explains multi-phase BOLD response. *Neuroimage* **268**, 119887 (2023).
35. Liang, F. et al. Sensory cortical control of a visually induced arrest behavior via corticotectal projections. *Neuron* **86**, 755–767 (2015).
36. Hu, F. & Dan, Y. An inferior-superior colliculus circuit controls auditory cue-directed visual spatial attention. *Neuron* **110**, 109–119.e3 (2022).
37. Xiong, X. R. et al. Interaural level difference-dependent gain control and synaptic scaling underlying binaural computation. *Neuron* **79**, 738–753 (2013).
38. Hind, J. E., Goldberg, J. M., Greenwood, D. D. & Rose, J. E. Some discharge characteristics of single neurons in the inferior colliculus of the cat. II. Timing of the discharges and observations on binaural stimulation. *J. Neurophysiol.* **26**, 321–341 (1963).
39. Tsytsarev, V. & Tanaka, S. Intrinsic optical signals from rat primary auditory cortex in response to sound stimuli presented to contralateral, ipsilateral and bilateral ears. *Neuroreport* **13**, 1661–1666 (2002).
40. Huberman, A. D. & Niell, C. M. What can mice tell us about how vision works?. *Trends Neurosci.* **34**, 464–473 (2011).
41. Prusky, G. T. & Douglas, R. M. Characterization of mouse cortical spatial vision. *Vis. Res.* **44**, 3411–3418 (2004).
42. Guru, A., Post, R. J., Ho, Y. Y. & Warden, M. R. Making sense of optogenetics. *Int. J. Neuropsychopharmacol.* **18**, pyv079 (2015).
43. Logothetis, N. K. Bold claims for optogenetics. *Nature* **468**, E3–E4 (2010).
44. Yizhar, O., Fenno, L. E., Davidson, T. J., Mogri, M. & Deisseroth, K. Optogenetics in neural systems. *Neuron* **71**, 9–34 (2011).
45. Tye, K. M. & Deisseroth, K. Optogenetic investigation of neural circuits underlying brain disease in animal models. *Nat. Rev. Neurosci.* **13**, 251–266 (2012).
46. Johnston, G. A. R. Muscimol as an ionotropic GABA receptor agonist. *Neurochem. Res.* **39**, 1942–1947 (2014).
47. Roth, B. L. DREADDs for neuroscientists. *Neuron* **89**, 683–694 (2016).
48. Takahashi, M. Morphological and electrophysiological characteristics of the commissural system in the superior colliculi for control of eye movements. *Prog. Brain Res.* **249**, 105–115 (2019).
49. Silva, A. C. & Koretsky, A. P. Laminar specificity of functional mri onset times during somatosensory stimulation. In: *Source* 99 (2002).
50. Gil, R., Fernandes, F. F. & Shemesh, N. Neuroplasticity-driven timing modulations revealed by ultrafast functional magnetic resonance imaging. *Neuroimage* **225**, 117446(2021).
51. Yu, X., Qian, C., Chen, D. Y., Dodd, S. J. & Koretsky, A. P. Deciphering laminar-specific neural inputs with line-scanning fMRI. *Nat. Methods* **11**, 55–58 (2014).
52. Jung, W. B., Ho Im, G., Jiang, H. & Kim, S.-G. Early fMRI responses to somatosensory and optogenetic stimulation reflect neural information flow. *Proc. Natl. Acad. Sci. USA* **118**, 2023265118 (2021).
53. Zong, W. et al. Large-scale two-photon calcium imaging in freely moving mice. *Cell* **185**, 1240–1256.e30 (2022).
54. Stosiek, C., Garaschuk, O., Holthoff, K. & Konnerth, A. In vivo two-photon calcium imaging of neuronal networks. *Proc. Natl. Acad. Sci.* **100**, 7319–7324 (2003).
55. Lake, E. M. R. et al. Simultaneous cortex-wide fluorescence Ca2+ imaging and whole-brain fMRI. *Nat. Methods* **17**, 1262–1271 (2020).
56. Schulz, K. et al. Simultaneous BOLD fMRI and fiber-optic calcium recording in rat neocortex. *Nat. Methods* **9**, 597–602 (2012).
57. Grienberger, C. & Konnerth, A. Imaging calcium in neurons. *Neuron* **73**, 862–885 (2012).
58. Albers, F., Wachsmuth, L., van Alst, T. M. & Faber, C. Multimodal functional neuroimaging by simultaneous bold fmri and fiber-optic calcium recordings and optogenetic control. *Mol. Imaging Biol.* **20**, 171–182 (2018).
59. Hu, G. et al. A developmental critical period for ocular dominance plasticity of binocular neurons in mouse superior colliculus. *Cell Rep.* **43**, 113667 (2024).
60. Russell, A. L., Dixon, K. G. & Triplett, J. W. Diverse modes of binocular interactions in the mouse superior colliculus. *J. Neurophysiol.* **127**, 913–927 (2022).
61. Hoy, J. L., Bishop, H. I. & Niell, C. M. Defined cell types in superior colliculus make distinct contributions to prey capture behavior in the mouse. *Curr. Biol.* **29**, 4130–4138.e5 (2019).
62. Schwartz, A. S. Electrophysiological correlates of flicker perception in the cat. *Physiol. Behav.* **8**, 603-609 (1972).
63. Schwartz, A. S. & Cheney, C. Neural mechanisms involved in the critical flicker frequency of the cat. *Brain Res.* **1**, 369–380 (1966).

64. Basso, M. A., Bickford, M. E., & Cang, J. Unraveling circuits of visual perception and cognition through the superior colliculus. *Neuron*, **109**, 918–937 (2021).
65. Schwartz, A. S. & Clark, G. Discrimination of intermittent photic stimulation in the rat without its striate cortex. *J. Comp. Physiol. Psychol.* **50**, 468 (1957).
66. Tabei, K. I. et al. Involvement of the extrageniculate system in the perception of optical illusions: a functional magnetic resonance imaging study. *PLoS One* **10**, e0128750 (2015).
67. Cowey, A. The blindsight saga. *Experimental Brain Research* **200**, 3–24 (2010).
68. Gale, S. D. & Murphy, G. J. Distinct cell types in the superficial superior colliculus project to the dorsal lateral geniculate and lateral posterior thalamic nuclei. *J. Neurophysiol.* **120**, 1286–1292 (2018).
69. Kaneda, K., Yanagawa, Y. & Isa, T. Transient enhancement of inhibition following visual cortical lesions in the mouse superior colliculus. *Eur. J. Neurosci.* **36**, 3066–3076 (2012).
70. De Franceschi, G. & Solomon, S. G. Visual response properties of neurons in the superficial layers of the superior colliculus of awake mouse. *J. Physiol.* **596**, 6307–6332 (2018).
71. Imas, O. A., Ropella, K. M., Ward, B. D., Wood, J. D. & Hudetz, A. G. Volatile anesthetics disrupt frontal-posterior recurrent information transfer at gamma frequencies in rat. *Neurosci. Lett.* **387**, 145–150 (2005).
72. You, T., Im, G. H. & Kim, S. G. Characterization of brain-wide somatosensory BOLD fMRI in mice under dexmedetomidine/isoflurane and ketamine/xylazine. *Sci. Rep.* **11**, 13110 (2021).
73. Airaksinen, A. M. et al. Simultaneous fMRI and local field potential measurements during epileptic seizures in medetomidine-sedated rats using RASER pulse sequence. *Magn. Reson Med*. **64**, 1191–1199 (2010).
74. Dinh, T. N. A., Jung, W. B., Shim, H. J. & Kim, S. G. Characteristics of fMRI responses to visual stimulation in anesthetized vs. awake mice. *Neuroimage* **226**, 117542 (2021).
75. Zhao, F., Zhao, T., Zhou, L., Wu, Q. & Hu, X. BOLD study of stimulation-induced neural activity and resting-state connectivity in medetomidine-sedated rat. *Neuroimage* **39**, 248–260 (2008).
76. Neves, D., Salazar, I. L., Almeida, R. D. & Silva, R. M. Molecular mechanisms of ischemia and glutamate excitotoxicity. *Life Sci.* **328**, 121814 (2023).
77. Raghavendra, M., Maiti, R., Kumar, S. & Acharya, S. Role of aqueous extract of Azadirachta indica leaves in an experimental model of Alzheimer's disease in rats. *Int J. Appl Basic Med Res*. **3**, 37 (2013).
78. Copeland, W. C. & K. B. Wallace. *Mitochondrial Genomics and Targeted Toxicities*. 1–15 (Elsevier, 2018).
79. Pai, S., Erlich, J. C., Kopec, C. & Brody, C. D. Minimal impairment in a rat model of duration discrimination following excitotoxic lesions of primary auditory and prefrontal cortices. *Front Syst Neurosci* https://doi.org/10.3389/fnsys.2011.00074. (2011)
80. Rosenquist, A. C., Ciaramitaro, V. M., Durmer, J. S., Wallace, S. F. & Todd, W. E. Ibotenic acid lesions of the superior colliculus produce longer lasting deficits in visual orienting behavior than aspiration lesions in the cat. *Prog. Brain Res*. **112**, 117–130 (1996).
81. Rosenquist, A. C., Ciaramitaro, V. M., Durmer, J. S., Wallace, S. F. & Todd, W. E. *Ibotenic Acid Lesions of the Superior Colliculus Produce Longer Lasting Deficits in Visual Orienting Behavior than Aspiration Lesions in the Cat*. vol. 112.
82. Baltes, C., Radzwill, N., Bosshard, S., Marek, D. & Rudin, M. Micro MRI of the mouse brain using a novel 400 MHz cryogenic quadrature RF probe. *NMR Biomed.* **22**, 834–842 (2009).
83. Watson, C. & P. G. *The Rat Brain in Stereotaxic Coordinates*. (2007).
84. Gil, R., Valente, M., Fernandes, F. & Shemesh, N. Evidence for a push-pull interaction between superior colliculi in monocular dynamic vision mode. *figshare. Dataset*. https://doi.org/10.6084/m9.figshare.28555010 (2025).

Acknowledgements

This study was funded in part by the European Research Council (ERC) (agreement No. 679058), as well as by Fundação para a Ciência e Tecnologia (Portugal), project 275-FCT-PTDC/BBB-IMG/5132/2014. The authors acknowledge the vivarium of the Champalimaud Centre for the Unknown, a facility of CONGENTO which is a research infrastructure co-financed by the Lisboa Regional Operational Programme (Lisboa 2020), under the PORTUGAL 2020 Partnership Agreement through the European Regional Development Fund (ERDF) and Fundação para a Ciência e Tecnologia (Portugal), project LISBOA-01-0145-FEDER-022170. R.G. thanks Fundação para a Ciência e Tecnologia for a Ph.D. fellowship PD/BD/128297/2017. The authors would also like to thank Dr. Cristina Chavarrías for the implementation of fMRI acquisition sequences.

Author contributions

N.S. and R.G designed the project and the necessary experiments and N.S. oversaw the implementation of the project. M.V. performed the lesions and histology. R.G. acquired the functional MRI data and performed all the data analysis. F.F.F. helped in the data analysis. N.S. and R.G. wrote the paper. N.S., R.G. and M.V. discussed the results and implications and commented on the manuscript at all stages.

Competing interests

The authors declare the following competing interest: Noam Shemesh serves on the Scientific Advisory Board of Bruker Biospin. The other authors declare no competing interests.

Additional information

Supplementary information The online version contains supplementary material available at https://doi.org/10.1038/s42003-025-08081-0.

Correspondence and requests for materials should be addressed to Noam Shemesh.

Peer review information *Communications Biology* thanks Yen-Yu Ian Shih, Xiaoqing Zhou and Yu Gu for their contribution to the peer review of this work. Primary Handling Editor: Christina Karlsson Rosenthal. A peer review file is available.

Reprints and permissions information is available at http://www.nature.com/reprints

Publisher's note Springer Nature remains neutral with regard to jurisdictional claims in published maps and institutional affiliations.

Open Access This article is licensed under a Creative Commons Attribution-NonCommercial-NoDerivatives 4.0 International License, which permits any non-commercial use, sharing, distribution and reproduction in any medium or format, as long as you give appropriate credit to the original author(s) and the source, provide a link to the Creative Commons licence, and indicate if you modified the licensed material. You do not have permission under this licence to share adapted material derived from this article or parts of it. The images or other third party material in this article are included in the article's Creative Commons licence, unless indicated otherwise in a credit line to the material. If material is not included in the article's Creative Commons licence and your intended use is not permitted by statutory regulation or exceeds the permitted use, you will need to obtain permission directly from the copyright holder. To view a copy of this licence, visit http://creativecommons.org/licenses/by-nc-nd/4.0/.

© The Author(s) 2025